Dissociation and dynamics of the high-vibrational-state HF molecules under intense half-cycle and few-cycle pulses

J. T. Lin* and S. H. Lin

Institute of Atomic and Molecular Sciences, Academia Sinica, P.O. Box 23-166, Taipei 10674, Taiwan

T. F. Jiang

Institute of Physics, National Chiao Tung University, 1001 Ta-Hsueh Road, Hsinchu 30010, Taiwan

This work explores the dissociation dynamics and angular distribution of the HF molecule interacting with intense half-cycle and few-cycle pulses, including the rotational degree of freedom. The dependences of the dissociation probability on both the pulse type and the pulse duration are discussed. Our results indicate that the angular distribution of the dissociation probability is highly asymmetric to the perpendicular direction of field polarization, and becomes more symmetric with an increase in the number of field cycles. The spatial distribution of the wave function demonstrates the feasibility of constructing a molecular wave packet by interacting with the half-cycle pulse.

PACS number(s): 42.50.Hz, 31.15.Qg, 31.70.Hq

I. INTRODUCTION

Strong and short laser pulses have been used in recent decades to examine the light-atom and -molecule dynamics over a wide range of laser frequencies. The experimental investigation of Jones *et al.* [1,2] ushered in an extensive study of the ionization and excitation of the Rydberg atom using a half-cycle pulse (HCP) [3–10]. The experiments were performed in the regime where the pulse duration T_p is in the order of the classical electron orbital period ($T_n = 2\pi n^3$) and the peak field strength E_m is in the order of the nuclear Coulomb field ($F_n = n^{-4}$) of the atom, where n denotes the principal quantum number of the Rydberg atom. (Atomic units are used hereafter unless stated otherwise.) This short and unidirectional electric-field pulse leads to several interesting results, such as the creation and probing of a wave packet [2], tracing of wave-packet trajectories, and the difference between n^{-1} scale ionization and microwave ionization or ramped dc electric-field ionization [1,4,10], etc.

The experimental results have led to numerous theoretical investigations using either quantum- or classical-mechanical approaches [8–10]. According to those investigations, the HCP experimental results can be interpreted classically by the interaction of the Rydberg atom with impulse field [1,9]. The quantum study of ionization correlates with the classical results over a regime where the time scale runs from the adiabatic limit ($T_p \gg T_n$) to the sudden ($T_p \ll T_n$) limit, and the ionization behavior changes from n^{-4} to n^{-1} scaling characteristics. However, the measured threshold field of ionization expressed as a function of pulse duration T_p lies on a universal, classical scaling invariant curve connecting the adiabatic and sudden regimes. Thus, the impulse field approximation is useful in the analysis of the atomic Rydberg state under the HCP excitations.

In contrast to the extensive amount of attention paid to atomic Rydberg states by the HCPs, corresponding studies on the molecular species are rare. Although incorporating rotational effects into the vibrational states complicates the calculation, experimental analogs have already been set up, such as field dissociation of molecular ions in the field-ion microscopy (FIM) and its passage through the high-field gap [11–13]. From the perspective of collision physics, HCP and one-cycle pulses [6] can imitate the interaction of atoms and molecules with a charged particle. Besides, advances in laser technology have made it possible for the frequent use of a time duration shorter than a single molecular rotational period in experiments. As widely anticipated, a pulse with a high intensity and duration comparable to the vibrational period will be contributed and controlled in the near future. Thus, this work elucidates the dynamics of the high-lying HF molecular vibrational states under HCP and few-cycle pulses while including the rotational effects. Results in this study provide further insight into such processes.

The rest of this paper is arranged as follows. We briefly introduce in Sec. II the numerical method of solving the time-dependent Schrödinger equation of an HF molecule under nonperturbative interaction. For different rotational states, the pseudospectral method is used to compute the eigenvalues and eigenfunctions with a Chebyshev basis. In Sec. III we present the results and discussions. The dissociation of HF by different pulses and duration are investigated therein. A summary is given finally.

II. MODEL AND CALCULATION

Under the Born-Oppenheimer approximation, the time-dependent Hamiltonian of light interaction with the molecule can be written as

$$\mathbf{H} = \mathbf{H}_0 - \vec{E}(t) \cdot \vec{d}(R),$$

$$\mathbf{H}_0 = \frac{\hat{P}_R^2}{2\mu} + \hat{V}_j(R),$$

(1)

---

*Present address: National Center for Theoretical Sciences, P.O. Box 2-131, Hsinchu 300, Taiwan.

$$\hat{V}_j(R) = D_e[e^{-2\alpha(R-R_o)} - 2e^{-\alpha(R-R_o)}]^2 + j(j+1)/(2\mu R^2),$$

where the parameters used are $D_e = 0.225, \alpha = 1.1741$, $R_o = 1.7329$, and reduced mass $\mu = 1744.8423$ for the HF molecule. The dipole moment function of HF is written as $\vec{d}(R) = p_a R \exp(-p_b R^4)\hat{R}$ with $p_a = 0.4541$ and $p_b = 0.0064$ [14,15]. This dipole function has an effective charge 0.31 at equilibrium position that was used by many authors in a simpler linear form [16–18].

The external field $\vec{E}(t) = E(t)\hat{z}$ used in this work is chosen to have the *sinusoidal* form

$$E(t) = E_m \sin\left(\frac{2\pi}{T_s}t\right), \quad 0 \leqslant t \leqslant N_p T_s, \quad N_p = 0.5, 1, 2, 3, \ldots. \tag{2}$$

When $N_p = 0.5$, the field is a half-cycle pulse, $N_p = 1$ is a one-cycle pulse, and so on. The total pulse duration is T_p ($= N_p T_s$). In our calculation, the maximum peak field strength E_m is fixed at 0.0338 (a.u.), which corresponds to the intensity of 4×10^{13} W/cm^2. Beyond this order of intensity, the ionization process will occur and the molecular potential with only one surface is inadequate to describe both dissociative and ionized processes.

The above time-dependent system is solved numerically by the split-operator algorithm [19–21]. We expand the wave function into partial waves:

$$\psi(R,\Omega;t) = \sum_{l=0}^{l_{max}} F_l(R;t) Y_{lm}(\Omega). \tag{3}$$

For the linearly polarized field, the magnetic quantum number m is conserved unless a magnetic field is added in, hence the system reduced into a two-dimensional one. The wave function is then propagated in time by alternating transformations between coordinate and momentum space by the fast-Fourier-transform method [22]. Additionally, the propagation of the dipole coupling term can be calculated through

$$e^{\pm ikd(R)\cos\theta} = \sum_{n=0}^{\infty} (\mp i)^n \sqrt{4\pi(2n+1)} j_n(kd(R)) Y_{n0}(\Omega). \tag{4}$$

By making the expansion

$$e^{\pm ikd(R)\cos\theta}\psi(R,\Omega;t) = \sum_{l=0}^{l_{max}} G_l(R;t) Y_{lm}(\Omega), \tag{5}$$

the time-dependent radial part becomes

$$\begin{aligned}
G_{l'}(R;t) = &\sum_{n=|l-l'|}^{n=l+l'} \sum_{l=0}^{l_{max}} (-1)^m (\pm i)^n (2n+1) \\
&\times \sqrt{(2l+1)(2l'+1)} j_n(kd(R)) \\
&\times F_l(R;t)(-1)^{2(l'-n)-m}(2l+1)^{-1/2} \\
&\times \langle l'0;n0|l0\rangle\langle l'-m;n0|l-m\rangle, \tag{6}
\end{aligned}$$

where $\langle l_1 m_1 l_2 m_2 | l_3 m_3 \rangle$ is the Clebsch-Gordan coefficient, $\Omega = (\theta, \phi), k = |E[t + (\Delta/2)]|\Delta$, and $j_n(kd(R))$ is the spherical Bessel function of order n. During the time evolution, the population probability of the system lies in the νth vibrational state. $P_\nu(t)$ is defined as

$$P_\nu(t) \equiv \sum_{j=0}^{j_{max}} P_{\nu j}(t), \tag{7}$$

where $P_{\nu j}(t) = |\langle \phi_{\nu j}(t) | \psi(t) \rangle|^2$ denotes the population of the jth rotational level associated with the νth vibrational bound state at time t and $\nu = 0,1,2, \ldots,23$, j runs from 0 to diminishing angular momentum j_{max}.

While the rovibrational coupling can be neglected, the separation of the rotational and vibrational degrees is a good approximation, and the wave function $\phi_{\nu j}$ can be written as a product of the radial part and the angular part, $\phi_\nu(R) Y_{jm}(\Omega)$, where $\phi_\nu(R)$ is the eigenfunction of the one-dimensional Hamiltonian $\hat{P}_R^2/2\mu + \hat{V}_0(R)$. When the system is in the highly rotational or vibrational states, this approximation is questionable and we have to include the centrifugal force in the potential. Chelkowski and Bandrauk expanded the potential around the minimum of the potential V_j and fitted them into a new Morse potential. The eigenfunctions are then solved from this new potential [23]. Instead of their method, we use the pseudospectral method [24–26] to solve the eigenfunction of $\mathbf{H}_0$ numerically and normalize the pseudocontinuous states within a box of length 46.0 a.u.. To compute the eigenfunctions, let $\phi_{\nu j}(R) \equiv \sqrt{f'}\chi_{\nu j}(x)$ with $R = f(x)$, and using Gauss-Chebyshev quadrature, we have

$$\chi_{\nu j}(x) = \sum_{i=1}^{N} g_i(x) \chi_{\nu j}(x_i), \tag{8}$$

where $g_i(x)$ is the cardinal function in the Chebyshev basis and $\{x_i\}_{i=0}^{i=N}$ are the collocation points and $g_i(x_k) = \delta_{ik}$.

By choosing $f(x) = L(1+x+C_1)/(1-x+C_2)$, where L, C_1, and C_2 are scaling factors which map R into the interval $[-1,1]$, the wave function satisfies the following equation:

$$\sum_{i=1}^{N} (\mathbf{H}_0)_{ki} \chi_{\nu j}(x_i) = E_{\nu j} \chi_{\nu j}(x_k), \tag{9}$$

where

$$(\mathbf{H}_0)_{ki} = -\frac{1}{2}\left(\frac{1}{f'(x_k)}\right)^2 \frac{d^2 g_i(x_k)}{dx^2} + V_j(x_k)\delta_{ki}, \tag{10}$$

with

$$-\frac{d^2 g_i(x_k)}{dx^2} = \begin{cases} \dfrac{(-1)^{i+k}(-x_k^2 - x_i x_k + 2)}{(1-x_k^2)(x_i - x_k)^2} & \text{if } k \neq i, \\[4mm] \dfrac{N^2-1}{3(1-x_i^2)} + \dfrac{1}{(1-x_i^2)^2} & \text{if } k = i. \end{cases} \tag{11}$$
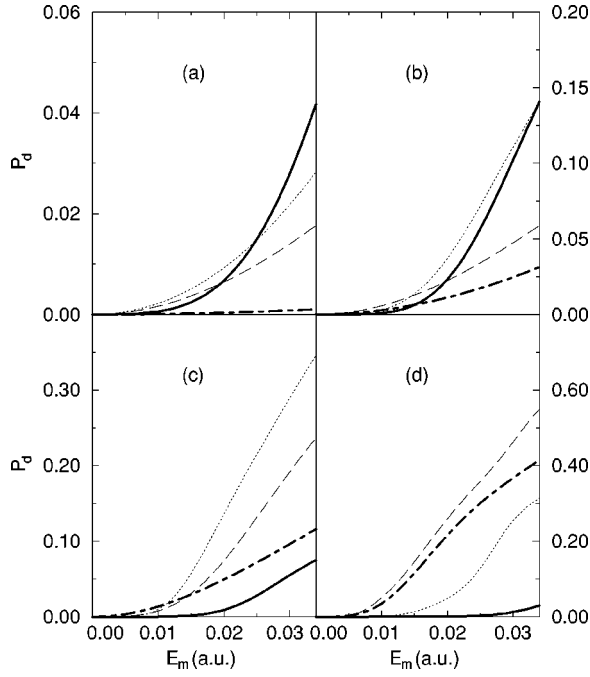
FIG. 1. The dissociation probabilities of the eighteenth vibrational excited state of HF against the field strengths E_m for different types of pulses specified by the number of field cycles N_p and durations T_p. The incident energy is the same for each case. Solid line is the HCP pulse ($N_p = 0.5$); dotted line is the one-cycle ($N_p = 1$) pulse; dashed line is the two-cycle ($N_p = 2$) pulse; and dotted-dashed line is the four-cycle ($N_p = 4$) pulse. (a) $T_p = 10$ fs for all types of pulses, (b) $T_p = 20$ fs, (c) $T_p = 40$ fs, (d) $T_p = 80$ fs. The dissociation features changed as T_p increased.

The dissociation probability $P_d(T_p)$ is calculated from the obtained eigenfunctions by

$$P_d(t) = 1 - \sum_{\nu=0}^{23} P_\nu(t)$$

$$= \int_{-1}^{1} P_d(\theta, t) d\cos\theta$$

$$= \int_{0}^{\infty} \sum_{j} P_j(\varepsilon_p, t) d\varepsilon_p$$

$$= \int_{0}^{\infty} P(\varepsilon_p, t) d\varepsilon_p, \tag{12}$$

where $P_d(\theta)$ is angular distribution of the dissociation probability and $P(\varepsilon_p)$ denotes the fragment energy spectra with j components $P_j(\varepsilon_p) = |\langle \phi_{\varepsilon_p, j} | \psi(t) \rangle|^2$, in which $\phi_{\varepsilon_p, j}$ is the eigenstate of $\mathbf{H}_0$ with eigenenergy $\varepsilon_p \geq 0$.

III. RESULTS AND DISCUSSIONS

In our calculation, radial coordinates of 2048 grid points with a range of 46 a.u. and an angular expansion of 10–45 partial waves are used. The population of the highest rotational state is less than 10^{-7} at the end of the pulse. In all cases of calculation, the norm of a wave function is accurate
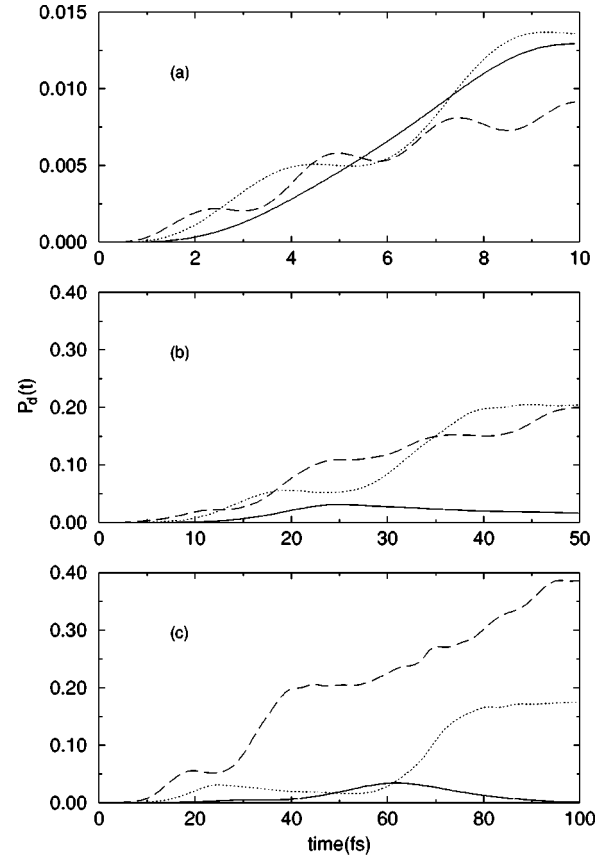

FIG. 2. The dissociation probabilities $P_d(t)$ as a function of time during the interaction at intensity $I = 4 \times 10^{13}$ W/cm^2. (a) $T_p = 10$ fs, (b) $T_p = 50$ fs, (c) $T_p = 100$ fs. The line types are the same as Fig. 1, i.e., solid line is for HCP and so on.

to the sixth decimal place during propagation, thus ensuring the reliability of our computational results even for a very small dissociation probability. When computing the eigenfunctions, all the vibrational bound states of $j = 0$ are generated with the eigenenergy accurate up to 10^{-8} in comparison with the exact eigenenergy of the Morse potential by using 256 grid points. The continuous states are also reproduced well by imposing only the boundary condition $\psi_{\nu j}(x_0) = 0$ and allowing the wave function to oscillate at the end point x_N. This approach differs from setting the wave function to zero at both ends, x_0 and x_N [24].

Herein, the initial state is prepared in the eighteenth excited state since the energy-level spacings in high vibrational states are much more closely spaced than the low-lying levels. Moreover, the linear combination of nearby states can construct a long-life wave packet.

A. Dissociation of HF by different pulse durations and number of cycles

Since the period of HF vibrational motion is about 10 fs, the dissociation of HF by different pulse durations around this time scale is of interest. Initially, calculations are performed for pulse durations ranging from 5 fs up to 300 fs. This pulse duration covers the time scale that is comparable to the vibrational period and the time duration that is long
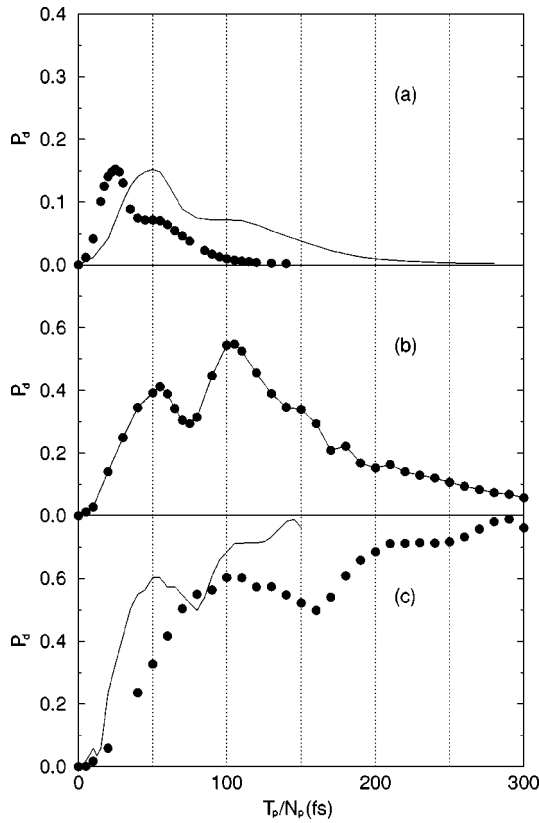
FIG. 3. The dissociation probabilities P_d against pulse durations T_p at intensity $I = 4 \times 10^{13}$ W/cm^2. (a) HCP, (b) one-cycle pulse, (c) two-cycle pulse. Solid line is the P_d vs scaled duration T_p/N_p, where $N_p = 0.5$ for the HCP pulse, $N_p = 1$ for the one-cycle pulse, and so on. Filled circles are P_d vs pulse duration T_p, not scaled. Note that the extreme dissociation probabilities (solid line) occur almost at the same position after duration scaling.

FIG. 4. Angular distribution of dissociation probability $P_d(\theta)$ for different pulse types and durations at intensity $I = 4 \times 10^{13}$ W/cm^2. The symbol for each pulse is the same as Fig. 1. (a) $T_p = 20$ fs for HCP and the one-, two-, and four-cycle pulses have the duration of 35 fs. All pulses have almost the same dissociation probabilities $P_d = 0.140$. (b) All types of pulses have the same pulse duration 50 fs but different dissociation probabilities P_d. The distribution $P_d(\theta)$ has been normalized by P_d for comparison such that $\int_0^\pi P_d(\theta)d\theta = 1$.

enough to smear out the short-time behavior. Figure 1 illustrates the dependence of dissociation probabilities on the number of field cycles and field strengths, where the pulse durations T_p ($= N_p T_s$) are 10, 20, 40, and 80 fs, and field cycles are HCP, one-cycle, two-cycle, and four-cycle, respectively. The total incident energy per unit area is $E_m^2 T_p/2$ for these pulses. Therefore, those pulses have the same incident energy and intensity as long as their durations T_p and peak field strengths E_m are equal, although their number of field cycles N_p and field period T_s may differ from each other. Figure 1(a) reveals that for $T_p = 10$ fs, the molecule has larger dissociation probabilities under HCP than under other types of pulses. A situation in which the pulse duration becomes longer, as shown in Figs. 1(c) and 1(d), suggests that the molecule becomes more easily dissociates with few-cycle pulses. This result can be understood from the impulse field approximation for short duration pulses, where the change of molecular energy can be approximated by $\Delta E(t) = (\vec{P} \cdot \vec{A} + \vec{A}^2/2)/\mu$ with $\vec{A} = -\int \vec{E}(t)dt$ and $\vec{P}$ is the initial momentum of molecule [1,2,4]. For a shorter duration pulse, a change in field direction cancels out the impulse integral and reduces the energy gain of a molecule. Hence, the dissociation probability is low. The unidirectional HCP provides a larger energy gain of the molecule because it does
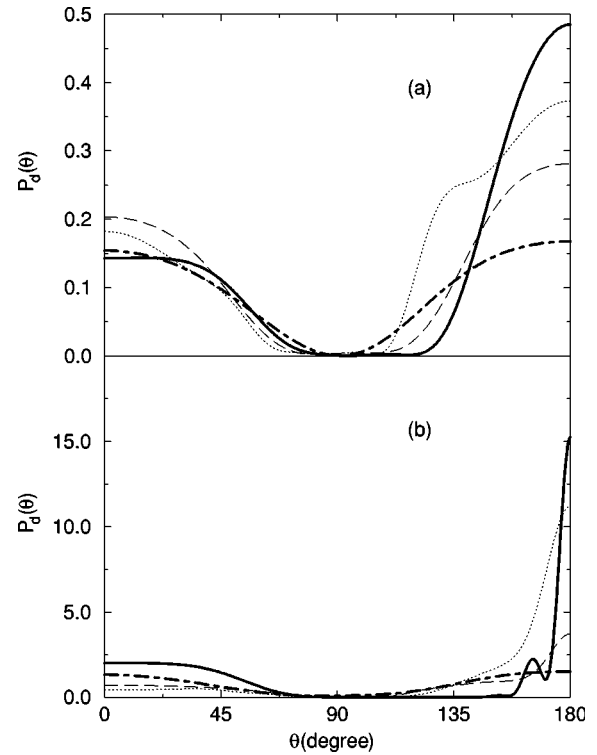
not change the field direction. As the pulse duration becomes longer than the molecular vibrational period, the total energy gain from the HCP pulse will be averaged out due to the back and forth motions of the system under the driving of the pulse field. On the other hand, for the few-cycle pulses, the periodic change of momentum may correlate with the molecular vibration and obtain net energy from each half-cycle of the pulse for longer duration pulses. This resonancelike effect does not occur in the HCP case. Consequently, the few-cycle pulses have larger dissociation probabilities than the HCP pulse for the longer duration pulses. In contrast to the anomalous ionization stability against the field strength of the surface-state electron (SSE) by HCP, the molecular rotations diminish the possibility of the wave function bouncing back and forth in the effective potential well formed by the external field and the Coulomb force. Instead of the anomalous stability, Fig. 1 reveals a monotonical increase of the dissociation probability against the external field strength for each fixed duration [27]. This is a distinct feature of molecular HCP excitations.

Figure 2 describes the dissociation history of different pulse types and durations under the same field strength as in Fig. 1. This figure indicates that the dissociation probability increases with time for a shorter HCP and, for a longer HCP,
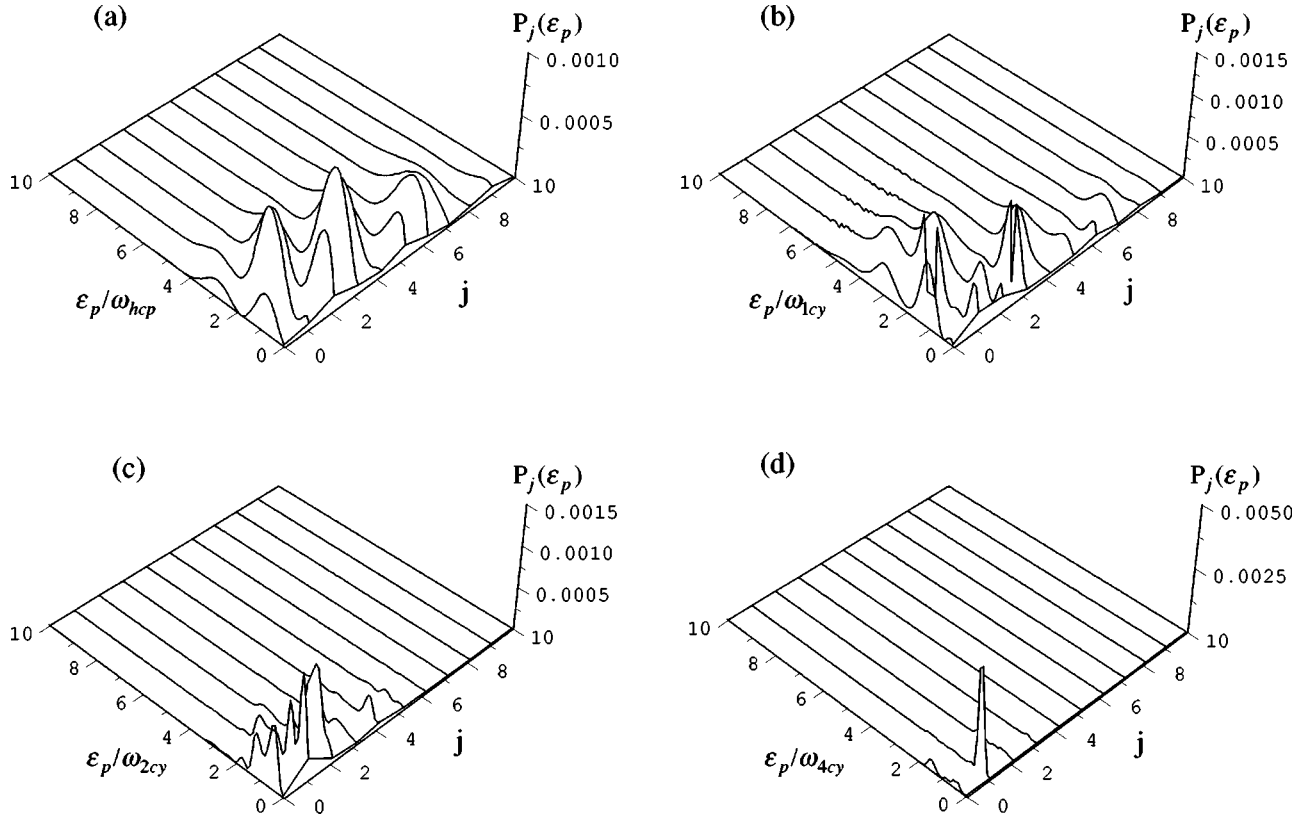
FIG. 5. The changes of fragment dissociation probability $P_j(\varepsilon_p)$ with respect to fragment energy ε_p and angular momentum j for each type of pulse in Fig. 4(a). The dissociation fragment energy ε_p is scaled by ω_{pulse}, where $\omega_{\text{pulse}} = 2\pi/T_s$ and the subscript ''pulse'' represents ''hcp'' for $N_p = 0.5$, ''1cy'' for one-cycle pulse, etc. All other parameters are the same as Fig. 4(a).

the probability initially increases and then decreases later. This phenomenon suggests that a loss of energy occurs as the wave packet bounces back. For the few-cycle pulses, the dissociation shows oscillatory structure over time and is smaller than the HCP case for shorter pulse duration, however it becomes larger than that of the HCP's as the duration increases. The above results can be understood in a manner similar to that in Fig. 1. An increase of intensity does not imply an increase of dissociation probability, since the dissociation probability depends on the pulse duration, field strength, and the pulse types.

Figure 3 illustrates the change of dissociation probabilities P_d with respect to the pulse duration T_p and field period T_s of the HCP, one-cycle, and two-cycle pulses. This figure clearly reveals several local maxima of P_d around some pulse durations. If the pulse duration is scaled by the number of field cycles, N_p, the local maxima of P_d occur roughly at the same field period T_s, indicating that the molecule tends to gain energy and dissociate at some special field period. The transition frequency of the 18th state to the 19th state is 3.844×10^{-3} a.u. Although the HCP and few-cycle pulses behave similarly to the quasistatic field, the Keldysh parameter $\gamma = \sqrt{D_e/U_p}$ for the HF molecule is substantially larger than 1 in our calculation due to the heavy mass in the ponderomotive potential $U_p = q_e^2 E_m^2/(4\mu\omega^2)$, where we choose $q_e = 0.31$ and $\omega = 2\pi/T_s$. This range of Keldysh parameter implies that the multiphoton process should be viewed as a more important process than tunneling in HF dissociation.

The above results suggest that all pulse types have near resonance frequency at scaled time 50 fs after the electric field is transformed into the frequency domain. For example, the 25 fs HCP has a 3.33×10^{-3} FWHM center at 3.43×10^{-3} and the 100 fs two-cycle pulse has a central frequency 3.07×10^{-3} with 9.1×10^{-4} bandwidth.

B. The fragment energy spectra and dissociation angular distribution

In the preceding section, we have demonstrated how the dissociation probability depends on the number of field cycles and pulse durations. This section examines the angular distribution of the dissociation probability and the fragment energy distribution defined in Eq. (12) for various types of pulses. Figure 4(a) indicates that the angular distribution of the dissociation probability P_d predominates when the molecular axis is in parallel with the field direction. In addition, this distribution is much smaller around the perpendicular direction than the parallel direction. Figure 4(b) also displays distributions but with different pulses. Notably, as the number of cycles increases, the angular distribution of P_d becomes more symmetric for both cases. This symmetry is due to the following reasons. An HCP drives the molecule around the field direction $-\hat{z}$ and dissociates the molecule in the $-\hat{z}$ direction during the interaction. Therefore, the dissociation probability centers asymmetrically around the $\hat{z}$ direction. On the other hand, the few-cycle pulses drive the wave packet back and forth, and the wave functions may
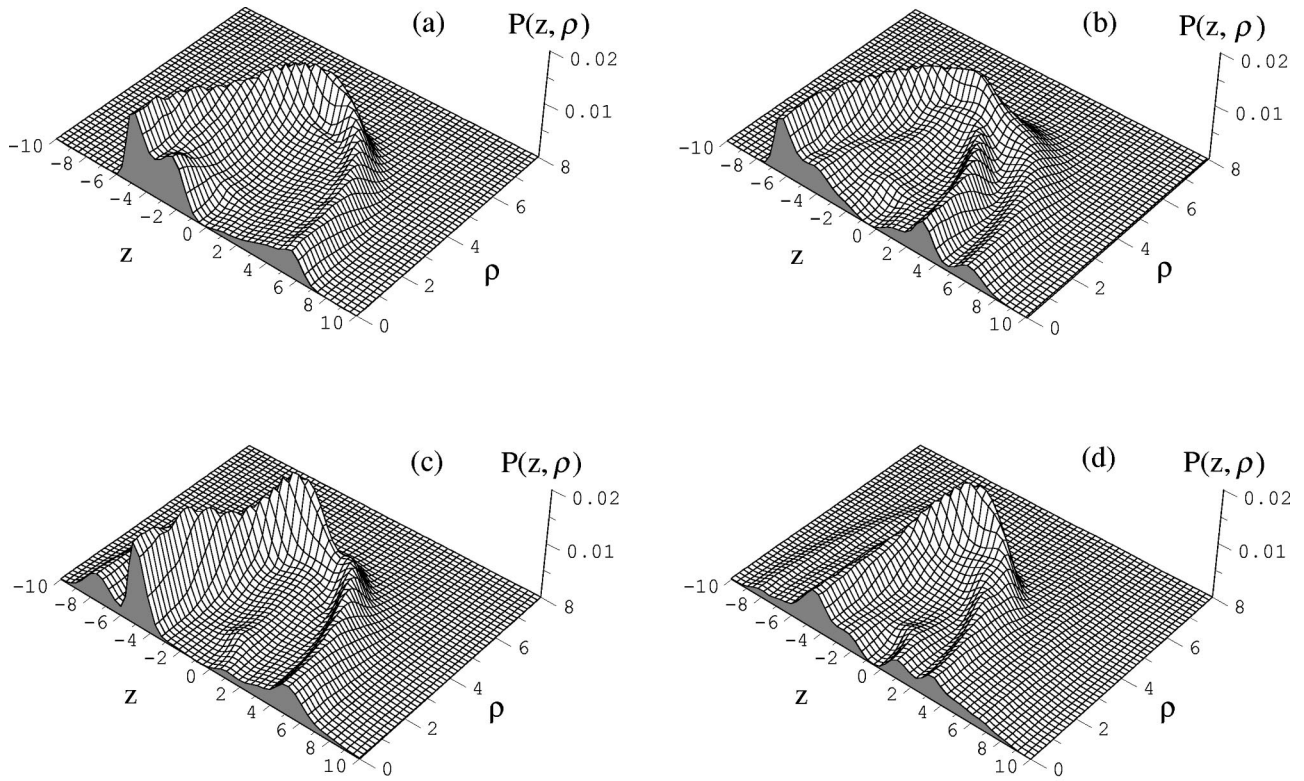
FIG. 6. Spatial probability density of wave functions in cylindrical coordinates at time T_p for Fig. 4(a). $P(z,\rho)=|\psi(z,\rho,T_p)|^2$ and z,ρ are in atomic units. (a) 20 fs HCP, (b) 20 fs one-cycle pulse, (c) 35 fs two-cycle pulse, (d) 35 fs four-cycle pulse.
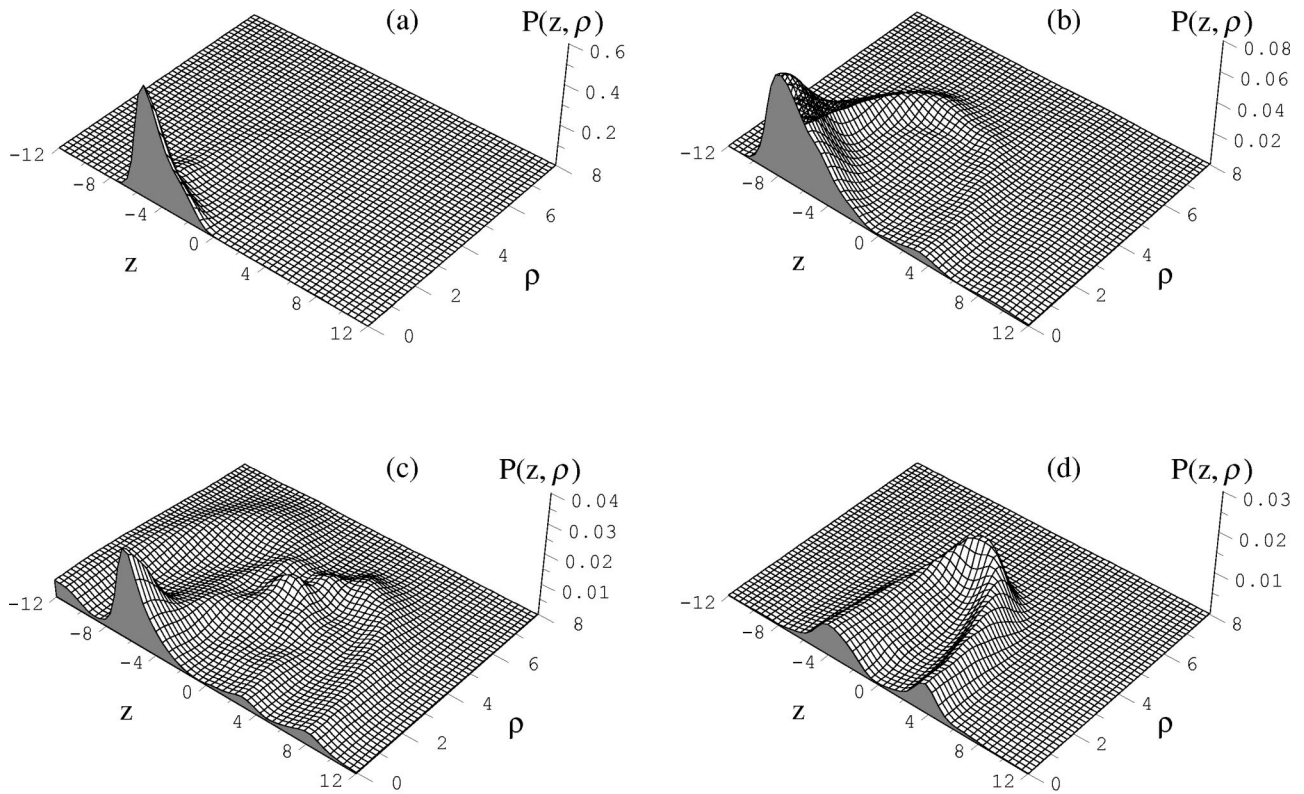

FIG. 7. Same as Fig. 6 except all parameters correspond to Fig. 4(b). (a) HCP, (b) one-cycle pulse, (c) two-cycle pulse, (d) four-cycle pulse. All pulses have the same duration $T_p=50$ fs.
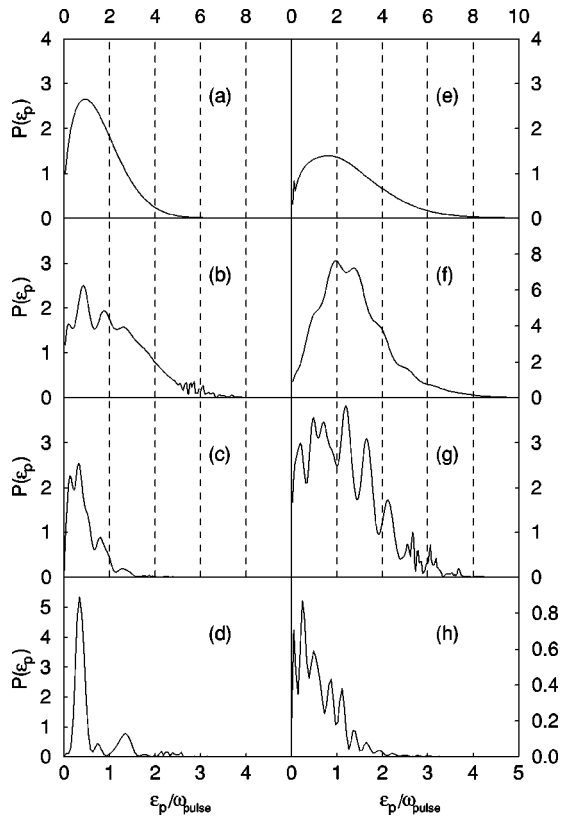
FIG. 8. The energy spectra of dissociation fragments $P(\varepsilon_p)$ vs energy ε_p, where ε_p has been scaled by ω_{pulse} as in Fig. 5. $P(\varepsilon_p)$ is summed over all j in Fig. 5. (a)–(d) have the same parameters as Figs. 4(a), 5, and 6. (e) and (f) have the same parameters as Figs. 4(b) and 7. The entire spectra signal has been magnified by a factor 10^3 and the abscissa scale of (d) and (h) differ from others.

spread over both the $+\hat{z}$ and $-\hat{z}$ directions. Consequently, our results reveal a more symmetric distribution around the $\hat{z}$ direction and the distribution slightly diffuses along the direction perpendicular to $\hat{z}$. Thus, we can infer that the pulse oscillation form affects the angular distribution of P_d and this should reflect on the angular momentum distribution of the dissociation signal. A higher asymmetric angular distribution should lead to higher angular momentum components in the dissociation signal. Therefore, Fig. 5 shows that the corresponding angular momentum components have the same field parameters as those in Fig. 4(a). The significant angular components of the dissociative fragment decrease as the number of cycles increases, and the fragment energy spectra of each angular component are narrower for the four-cycle case than those for the HCP pulse. This is due to the fact to that the dissociation angular distribution is more symmetric and the pulse bandwidth is narrower for a pulse with a larger number of field cycles.

Figures 6 and 7 present the spatial distribution of wave functions at the end of the interaction in the cylindrical coordinates. The field parameters correspond to those of the cases in Figs. 4(a) and 4(b), respectively. According to our results, the spatial probability also reveals the spatial asymmetric effect of the HCP pulse. From the above discussions we believe that *a less oscillatory pulse is preferred when constructing a spatial localized wave packet.* The less oscillatory pulse implies a broader frequency band, resulting in a wider angular momentum population distribution over accessible angular components. This enhances the feasibility of constructing a molecular wave packet by on HCP.

Figure 8 shows the energy spectra of fragments. For the HCP case, the spectrum is broad banded and the pulse drives the system away unidirectionally. On the other hand, the four-cycle pulse drives the system back and forth and the fragment spectra show a more complicated structure as in the $P_d(t)$ of Fig. 2. Notably, the energy peaks become clearer as the pulse duration increases. This is due to the fact to that the system has a longer time to react with the oscillatory driving field. Consequently, the fragment energy spectra display a similar pattern to that of the above-threshold dissociation (ATD) spectra, although the peaks are not totally evenly spaced.

IV. CONCLUSION

This work has studied how the pulse duration, number of field cycles of the HCP, and few-cycle pulses affect the dissociation of the HF molecule high-lying vibrational states. Our results indicate that the classical impulse approach should be a good approximation for the HF molecular dissociation when the HCP pulse duration is comparable to the order of the vibrational time scale of the molecule. Besides, the angular distribution of the dissociative flux along the electric-field axis exhibits the molecular alignment with the field direction. Studying the phenomena of molecular wave packet dynamics and its dissociation by the HCP with the one-dimensional potential [28,29] is worthwhile. However, for realistic considerations, full dimensional investigation is necessary. From the localization of the angular distribution of the dissociation probability, this investigation demonstrates the feasibility of creating a molecular wave packet in three-dimensional form. The exploration of the construction of such a wave packet and its evolution dynamics with or without external field is currently under investigation.

[1] R.R. Jones, D. You, and P.H. Bucksbaum, Phys. Rev. Lett. **70**, 1236 (1993).

[2] R.R. Jones, Phys. Rev. Lett. **76**, 3927 (1996).

[3] G.M. Lankhuijzen, and L.D. Noordam, Phys. Rev. Lett. **74**, 355 (1995).

[4] C. Raman, C.W.S. Conover, C.I. Sukenik, and P.H. Bucksbaum, Phys. Rev. Lett. **76**, 2436 (1996).

[5] P. Kristensen, G.M. Lankhuijzen, and L.D. Noordam, J. Phys.

B **30**, 1482 (1997).

[6] T.J. Bensky, G. Haeffler, and J.J. Jones, Phys. Rev. Lett. **79**, 2018 (1997).

[7] C.W.S. Conover and J.H. Rentz, Phys. Rev. A **55**, 3787 (1997).

[8] T.F. Jiang and C.D. Lin, Phys. Rev. A **55**, 2172 (1997).

[9] C.O. Reinhold, H. Shao, and J. Burgdörfer, J. Phys. B **27**, L469 (1994).

[10] S. Yoshida, C.O. Reinhold, and J. Burgdörfer, Phys. Rev. A **58**, 2229 (1998).

[11] T.T. Tsong, Phys. Rev. Lett. **55**, 2826 (1985).

[12] T.T. Tsong and M.W. Cole, Phys. Rev. B **35**, 66 (1987).

[13] A.C. Riviere and D.R. Sweetman, Phys. Rev. Lett. **5**, 560 (1960).

[14] R.C. Brown and R.E. Wyatt, J. Chem. Phys. **90**, 3590 (1986).

[15] M. Kaluža, J.T. Muckerman, P. Gross, and H. Rabtiz, J. Chem. Phys. **100**, 4211 (1994).

[16] S. Chelkowski, A.D. Bandrauk, and P.B. Corkum, Phys. Rev. Lett. **65**, 2355 (1990).

[17] J.T. Lin, T.L. Lai, D.S. Chuu, and T.F. Jiang, J. Phys. B **31**, L117 (1998).

[18] J.T. Lin, D.S. Chuu, and T.F. Jiang, Phys. Rev. A **58**, 2337

(1998).

[19] M.D. Feit, J.A. Fleck, Jr., and A. Steiger, J. Comput. Phys. **47**, 412 (1982).

[20] M.R. Hermann and J.A. Fleck, Jr., Phys. Rev. A **38**, 6000 (1988).

[21] T.F. Jiang and S.I. Chu, Phys. Rev. A **46**, 7322 (1992).

[22] M.D. Feit and J.A. Fleck, Jr., J. Chem. Phys. **80**, 2578 (1984).

[23] S. Chelkowski and A.D. Bandrauk, J. Chem. Phys. **99**, 4279 (1993).

[24] J. Wang, S.I. Chu, and C. Laughlin, Phys. Rev. A **50**, 3208 (1994).

[25] D. Gotlieb and S. Orszag, *Numerical Analysis of Spectral Methods: Theory and Applications* (SIAM, Philadelphia, 1977).

[26] J.P. Boyd, *Chebyshev and Fourier Spectral Methods* (Springer-Verlag, New York, 1989).

[27] T.F. Jiang, Phys. Rev. B **55**, 4238 (1997). We thank Professor C.D. Lin for helpful discussions on this point.

[28] J.A. Yeazell and C.R. Stroud, Jr., Phys. Rev. A **43**, 5153 (1991).

[29] R.B. Bernstein and A.H. Zewail, J. Chem. Phys. **90**, 829 (1989).